JOURNAL OF GUIDANCE, CONTROL, AND DYNAMICS
Vol. 31, No. 3, May–June 2008

Rate-Dependent Elastoslide Model for a Magnetorheological Damper

Wei Hu* and Norman M. Wereley†
University of Maryland College Park, Maryland 20742

DOI: 10.2514/1.32732

A rate-dependent elastoslide model is developed to study the quasi-steady and dynamic behavior of a magnetorheological damper. This time-domain model uses a rate-dependent slide and a parallel viscous damping to describe the practical yield behavior demonstrated by field-activated magnetorheological fluids, and it uses a stiff spring in series with the slide to represent the preyield stiffness of the damper. A method of determination of the model parameters is developed using single-frequency hysteresis data of the magnetorheological damper. The model parameters are determined using virtual loading curves identified from the force-displacement and force-velocity hysteretic diagrams. A relationship between current controllable parameters and current input is established. The fidelity of the model is justified by a good correlation between modeling results and experimental steady-state data over a broad amplitude and moderate-frequency range. Significantly, this model captures nonlinear amplitude- and frequency-dependent behavior of magnetorheological dampers using constant model parameters and trivial computational effort.

I. Introduction

MAGNETORHEOLOGICAL (MR) fluids are materials that change their rheological behavior in the presence of an applied magnetic field. The substantial field-induced yield stresses exhibited by MR fluids can change their apparent viscosity very rapidly with the application of magnetic field, and MR fluids can be easily activated using standard circuit-board dc power sources. Although the quasi-steady behavior of the MR valve or damper can be described by a simple Poiseuille flow analysis, as in [1–3], the hysteresis behavior demonstrated by the MR valve under a sinusoidal loading cannot be sufficiently captured by the analysis. Because the MR valve may operate in dynamic or transient loading conditions, prediction of dynamic behaviors is important to evaluate the performance of the MR valve.

Quasi-steady modeling using the Bingham-plastic constitutive model for the MR fluids [1,4] was extended to describe the behavior of the MR damper under oscillatory sinusoidal loading conditions [5,6]. The nonlinear Bingham model can be represented by a viscous damping and a Coulomb friction element in parallel, but it cannot describe the progressive and continuous preyield behavior that is observed in the test data of MR dampers. On the other hand, the biviscous model [7,8] and the Eyring-plastic model [9] use piecewise or continuous functions to represent preyield and postyield viscosities, but neither biviscous nor Eyring models can be used to describe the force-velocity hysteresis behavior.

Generally, phenomenological modeling methods have been used to capture the preyield force-velocity hysteresis. The hysteretic biviscous model developed by Pang et al. [5] and Wereley et al. [10] is a combination of several piecewise continuous functions, and the force-velocity hysteresis can be reconstructed using these functions. Choi et al. [11] developed a single hysteretic function to describe the low-speed hysteresis characteristics of the MR isolator, and this model was shown successfully in control applications. In addition, a polynomial model proposed by Choi et al. [12] employed a polynomial to fit the force-velocity hysteresis loop. All of these models employ mathematical functions instead of mechanical elements to capture the force-velocity hysteresis. Alternatively, Kamath et al. [13] developed a mechanism-based, nonlinear, piecewise-smooth, viscoelastic-plastic model. This model consists of a viscoelastic element for preyield behavior and a viscous element for postyield behavior, between which a nonlinear shape function describes the smooth transition between preyield viscoelastic and postyield viscous behaviors. As an extension of the Bingham-plastic model, Gamota and Filisko [14] proposed a model given by a Bingham model in series with a standard linear solid model. All of these models can describe the postyield and preyield behaviors of MR dampers. However, these models only phenomenologically describe the hysteresis using some shape functions and do not reflect the physical yield mechanism in the MR damper. As a result, this type of modeling generally leads to amplitude- and frequency-dependent model parameters. To implement the damper model, the excitation amplitude and frequency have to been known a priori, which is inconvenient when predicting the response under complex loading conditions.

An exception for hysteretic modeling is the Bouc–Wen model [15], which has proven to be successful in numerical modeling of a hysteretic system under random excitation. Based on the Bouc–Wen model, a generalized hysteresis model was proposed by Spencer et al. [16]. The model parameters were determined to best fit the data (including step response, constant voltage/random displacement, and random displacement with random voltage), and so the hysteretic behavior of the damper under step and random loading was predicted very well using this modified 14-parameter Bouc–Wen model. However, the detailed relationship between model parameters and excitation amplitude and frequency was not shown. Also, the physical interpretation of the Bouc–Wen model parameters is tenuous at best, and the model structure is quite complicated.

In addition, a fluid mechanics approach was used by Wang and Gordaninejad [17] to develop a theoretical model for predicting the behavior of MR dampers. In this model, the fluid compressibility was considered and a Herschel–Bulkley constitutive equation was used for the MR-fluid behavior. The major advantage of this model is its dependency on only the geometric and material properties of the device. However, this approach was validated using a double-ended rod damper, and it becomes very complicated for dampers with accumulators or gas chambers, leading to higher computational cost. Similarly, Hong et al. [18] developed a model with lumped mechanical and fluid elements. This hydromechanical model

Received 10 June 2007; revision received 9 November 2007; accepted for publication 13 November 2007.

*Research Associate, Alfred Gessow Rotorcraft Center, Department of Aerospace Engineering; weihu@umd.edu. Member AIAA.

†Professor, Alfred Gessow Rotorcraft Center, Department of Aerospace Engineering; wereley@umd.edu. Associate Fellow AIAA.

consists of physically motivated hydromechanical lumped parameters to represent fluid inertia, damping, yield force, and compliances associated with MR dampers. The preyield hysteresis force behavior of the MR damper was well-represented by this model, but all model parameters were dependent on the applied field and excitation frequency.

Based on the Bingham-plastic material model for the MR fluids, a rate-dependent elastoslide model is developed in this paper to study the quasi-steady and dynamic behavior of the MR-fluid-based damper. This time-domain model uses a rate-dependent slide in parallel with a viscous damping mechanism to represent practical yield behavior of MR fluids, and it uses a stiff spring in series with the slide to reflect the preyield stiffness due to fluid compressibility. A method of identifying model parameters is developed using single-frequency hysteresis data of the MR damper. The model parameters are determined using virtual initial loading curves identified from the force-displacement and force-velocity hysteretic diagrams. A relationship between current controllable parameters and the corresponding current input is approximated using determined parameter at different currents.

II. Experimental Characterization

A. Experimental Setup

To evaluate the proposed rate-dependent elastoslide model, dynamic tests with steady-state sinusoidal excitations are conducted on two identical MR linear stroke dampers. A schematic of the nominal MR damper is shown in Fig. 1. The hydraulic cylinder houses the damper piston, in which a magnetic circuit is mounted. At the base and inside the hydraulic cylinder is a nitrogen accumulator. The accumulator is used to compensate for changing rod volume in the hydraulic cylinder, as well as thermal expansion of the MR fluid, and to prevent cavitation on the low-pressure side of the piston in the MR damper. The MR fluid in the damper flows through an annular gap in the piston head, wherein it can be activated by a current applied to the magnetic circuit.

The configuration of the experimental setup is shown in Fig. 2. The MR damper is tested on an MTS 810 24.466-kN (5000-lb)

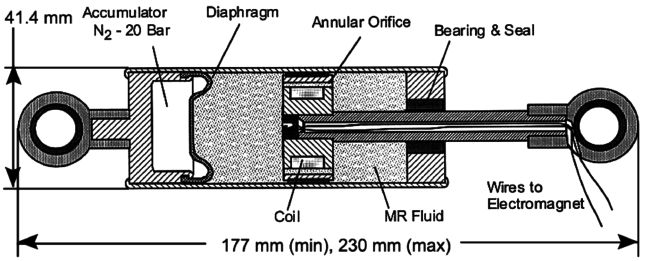

Fig. 1 Schematics of the MR damper.

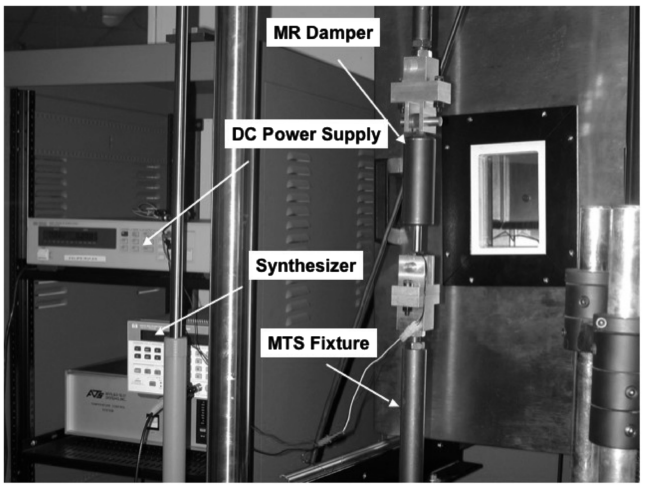

Fig. 2 Test setup for the MR damper.

Table 1 Dual-frequency test matrix

		5-Hz amplitude, mm				
		0.5	1	1.5	2.5	Current, A
2.5-Hz amplitude, mm	0.5	×	×	×	×	0–0.3
	1.0	×	×	×	×	0–0.3
	1.5	×	×	×	×	0–0.2
7.5-Hz amplitude, mm	0.5	×		×	×	0–0.2
	1.0	×		×	×	0–0.2

servohydraulic material testing machine. A displacement linear variable differential transformer (LVDT) sensor is used for displacement measurement and a load cell is used for measuring the force. The machine can be operated in two ranges for displacements of 127 and 12.7 mm (5 and 0.5 in.) and forces of 24.466 kN and 2.4466 KN (5000 and 500 lb). Fixtures and grips are designed to hold the damper in place. A dc power supply is used to provide current control during testing. The normal range of the applied current is between 0 and 1.5 A, and the maximum applied voltage is 10-V dc. An HP 8904A multifunction synthesizer is used to generate and sum the sinusoidal signals for dual-frequency tests.

The MR damper characteristics are determined using various harmonic inputs when the damper is energized with 0, 0.1, 0.2, and 0.3 A of applied current. The harmonic frequency is chosen to be appropriate for a helicopter rotor system at $\Omega_{\text{pri}} = 7.5$ Hz (the baseline 1/rev frequency), $\Omega_{\text{lag}} = 5.0$ Hz (the lag/rev frequency), and $\Omega_{\text{com}} = 2.5$ Hz (the lower harmonic of lag/rev and 1/rev frequencies). All experimental results are obtained at room temperature (25°C). The steady-state dynamic tests for both MR dampers consist of single-frequency and dual-frequency tests. For single-frequency tests, the shaft of the damper is excited using sinusoidal displacement at amplitudes from 0.25 to 4 mm and at three different frequencies of Ω_{pri}, Ω_{lag}, and Ω_{com}, respectively. The single-frequency force-displacement and force-velocity data are used to determine the model parameters and evaluate the fidelity of the model. For dual-frequency tests, two dual-frequency combinations (2.5 Hz/5 Hz and 5 Hz/7.5 Hz) are used to evaluate the adaptability of the model in multifrequency loading conditions. The dual-frequency experimental matrix is shown in Table 1.

B. Experimental Results

During each test, a data acquisition sampling rate of 2048 Hz is chosen, and 10 to 20 cycles of force and displacement data are measured. To reduce the noise of the sinusoidal displacement signal, a Fourier series is used to reconstruct the input displacement. The reconstructed displacement signal is then differentiated to obtain the velocity data. The Fourier series expansion of the input displacement is

$$x(t) = \frac{x_0}{2} + \sum_{k=1}^{\infty} [X_{c,k} \cos(k\omega t) + X_{s,k} \sin(k\omega t)] \tag{1}$$

where

$$X_{c,k} = \frac{\omega}{\pi} \int_0^{\frac{2\pi}{\omega}} x(t) \cos(k\omega t)\, \mathrm{d}t, \qquad X_{s,k} = \frac{\omega}{\pi} \int_0^{\frac{2\pi}{\omega}} x(t) \sin(k\omega t)\, \mathrm{d}t \tag{2}$$

For single-frequency testing, any bias and higher harmonics are filtered, so that only the frequency of interest remains in which $\omega = \Omega_{\text{pri}}$, Ω_{lag}, and Ω_{com}, respectively. The displacement is reconstructed using only the first harmonic as

$$x(t) = X_c \cos(\omega t) + X_s \sin(\omega t) \tag{3}$$

For dual-frequency testing, the HP 8904A multifunction synthesizer is used to generate and sum the sinusoidal signals for both frequencies. The general equation for the input dual displacement signal is written as

$$x(t) = A_{\text{lag}} \sin(\Omega_{\text{lag}} t) + A_{\text{com}} \sin(\Omega_{\text{com}} t) \tag{4}$$

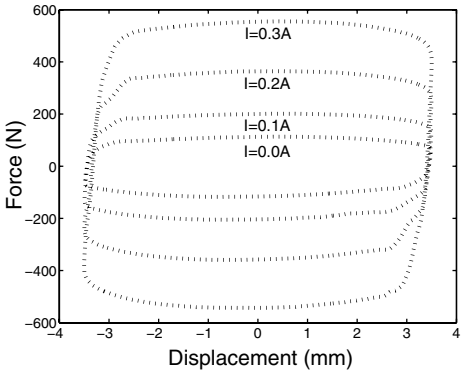

a) Force-displacement diagram

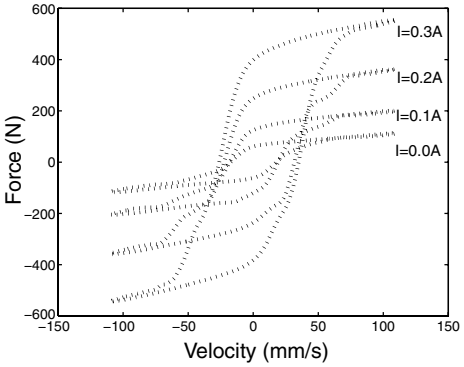

b) Force-velocity diagram

Fig. 3 Hysteresis cycles for the MR damper.

and

$$x(t) = A_{\text{lag}} \sin(\Omega_{\text{lag}} t) + A_{\text{pri}} \sin(\Omega_{\text{pri}} t) \tag{5}$$

The signal is periodic, with a frequency corresponding to the highest common factor of both harmonics (i.e., 2.5 Hz). The displacement signal is filtered using $\omega = 2.5$ Hz as the base frequency. The first three harmonics are needed to reconstruct the dual-frequency displacement signal. Because the MR damper produces nonlinear damping force, the measured force is not filtered. However, to reduce the offset in the measured force due to the presence of the accumulator, the measured bias force is subtracted using the bias term in the Fourier series of the force.

Typical force-displacement hysteresis data are shown in Fig. 3a, in which the force-displacement diagram was obtained using a sinusoidal displacement excitation at $\Omega_{\text{lag}} = 5$ Hz with an amplitude of 3.5 mm. Four different currents of 0, 0.1, 0.2, and 0.3 A are applied to the MR damper. From the force-vs-displacement cycles, damping is proportional to the area enclosed by a force-displacement hysteresis cycle, which is the energy dissipated by the MR damper. The typical effect of the applied current shown in the hysteresis cycles is the increment of the steep area close to zero velocity (shown at the maximum displacement), such that the enclosed hysteresis area is enlarged. This implies that the damping effect of the MR damper is obtained by the friction effect or yield process of the MR fluid flowing through the annular gap in the piston head. Similarly, the force-velocity diagram of the MR damper shown in Fig. 3b demonstrates a Bingham or yield behavior, and the force-velocity hysteretic behavior results from a preyield spring or compression effect.

To demonstrate the damping-augmentation effect quantitatively, a standard linearization technique, equivalent viscous damping, is used to characterize the MR damper when under a sinusoidal loading:

$$x = X_0 \sin(\Omega t + \phi) \tag{6}$$

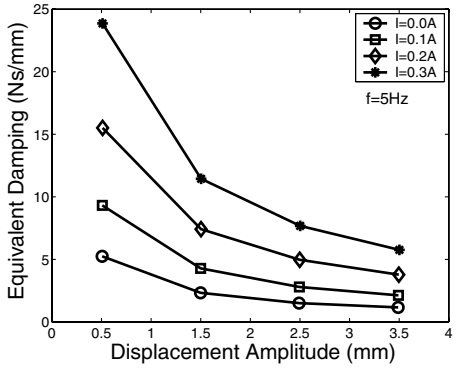

Fig. 4 Linear damping characterization of the MR damper.

The analytical damping force $F(t)$ is assumed to be proportional to the damper shaft velocity $\dot{x}(t)$, as

$$F(t) = C_{\text{eq}} \dot{x}(t) \tag{7}$$

With experimental damper force data f, the equivalent viscous damping C_{eq} is computed by calculating the energy dissipated over a cycle E at frequency Ω, using

$$E = \oint f(t)\,\mathrm{d}x = \int_0^{\frac{2\pi}{\Omega}} f(t)\dot{x}(t)\,\mathrm{d}t \tag{8}$$

and equating the dissipated energy of the damper to that of an equivalent viscous damper:

$$C_{\text{eq}} = \frac{E}{\pi \Omega X_0^2} \tag{9}$$

where X_0 is the amplitude of the displacement excitation. Thus, the damping characteristic of the MR damper at different amplitudes and currents can be demonstrated using equivalent viscous damping, as shown in Fig. 4. Clearly, the equivalent viscous damping of the MR damper is a nonlinear function of excitation amplitude, which is different from what one would expect for a linear viscous damper. However, the significant advantage of the MR damper is that the equivalent damping can be varied over a wide range as the applied current is varied.

The equivalent viscous damping is a linear characterization method that can be used to determine the damping capacity of the MR damper, but it cannot be used to predict the nonlinear forced response of the MR damper. Therefore, a rate-dependent elastoslide damper model is developed to capture the nonlinear damper behavior, and the model performance is evaluated by comparison between experimental and predicted damper response under varied loading conditions.

III. Evaluation of a Rate-Dependent Elastoslide Model

The proposed rate-dependent elastoslide model (RDES) is shown in Fig. 5, which is composed of a rate-dependent elastoslide element to describe the yield behavior of MR dampers, a parallel postyield viscous damping, and a parallel soft spring to reflect the stiffness effect of the accumulator. The composition of the model is similar to the Bouc–Wen model, but the Bouc–Wen element is instead replaced with a physically motivated elastoslide mechanism. It will be shown that this simple elastoslide element is appropriate for the yield behavior of MR-fluid-based dampers and that the rate-dependent elastoslide model captures most nonlinear characteristics of MR dampers.

Because the MR fluid is characterized by the Bingham-plastic model, a force-velocity relationship is derived on the basis of a flow-mode damper. Because this ideal relationship does not include the effect of practical fluid bleed in the damper, the Bingham damper model cannot describe the transition behavior from preyield to postyield. Thus, extended from the Bingham model mechanisms, the rate-dependent elastoslide element is physically interpreted. The

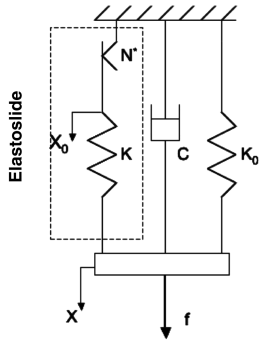

Fig. 5 Rate-dependent elastoslide model.

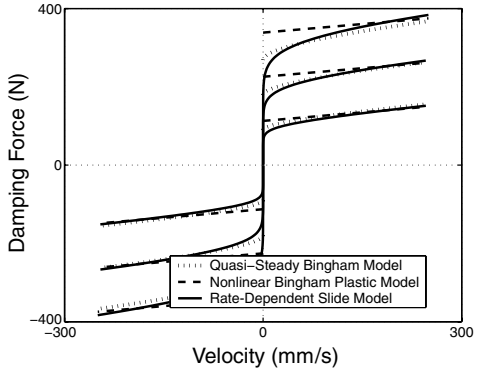

Fig. 6 Quasi-static force-velocity relationship predicted by MR models.

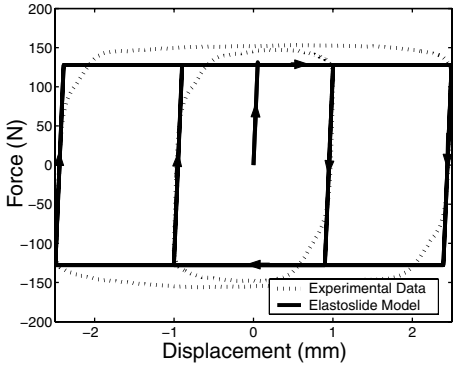

Fig. 7 Hysteresis behavior of an elastoslide model.

numerical implementation of the model is discussed. A suitable slide function is found to avoid a stiff numerical problem. The identification procedure for the model parameters is also given in this section.

A. Rate-Dependent Slide

The quasi-steady behavior of MR dampers is well understood by the analysis using MR fluid constitutive model and damper geometry [1,2,19]. For a flow-mode damper with a steady shaft velocity, the damping force is developed because of the pressure drop through the annular gap within the cylindrical MR damper body. According to the quasi-steady flow analysis [1], the ideal relationship between damper force F and shaft velocity v is derived as

$$F = \frac{C_0}{(1-\bar{\delta})^2(1+\frac{\bar{\delta}}{2})} v \tag{10}$$

where C_0 is the Newtonian damping coefficient for the field-off MR damper, and $\bar{\delta}$ is the nondimensional plug thickness, which is a function of yield force and shaft velocity. From Eq. (10), the ideal quasi-steady force-velocity plots are shown as dotted lines in Fig. 6. Analytically, before the damper force reaches a certain yield force, the MR fluid in the valve of the damper cannot flow. Thus, there is an abrupt jump in force from preyield solid to postyield Newtonian flow at small velocities, and the yield force is a function of the applied field. It was shown in [20] that Eq. (10) can be approximated by a linear summation of a field-controlled yield force and a postyield Newtonian force:

$$F = F_y + C_0 v \tag{11}$$

This is the Bingham-plastic damper model. Because the approximation works best in the high-speed postyield region, the Bingham-plastic model inherently cannot predict damper force accurately, especially over the transition region from preyield to postyield.

The macrobehavior of the damper predicted by both quasi-steady analysis and the Bingham-plastic damper model presents a rigid preyield region, which is exactly the behavior of a Coulomb slide. However, the piston bleed or blow-by of fluids between the piston and cylinder in a practical MR damper results in a preyield slip between the preyield and postyield phases in the force-velocity curve. Thus, to render the Coulomb slide, a rate-dependent slide model can be used to describe the nonlinear damping behavior in the preyield, or low-velocity, region. Taking numerical feasibility into consideration, a fractional power function of velocity is feasible to simulate both preyield and postyield behaviors of the force-velocity curve; that is,

$$N^* = N\left(\frac{v}{v_r}\right)^{\frac{1}{p}} \tag{12}$$

where N is the field-dependent yield force, p is a positive odd integer, and v_r is a constant reference velocity at which the slide transitions from the preyield region to the postyield region. The force-velocity relationship described by the rate-dependent slide model combined with a postyield viscous damping is shown as solid lines in Fig. 6. Compared with the nonlinear Bingham-plastic model, the rate-dependent slide demonstrates significant improvement in describing the force-velocity relation over a broad velocity and yield-stress range.

B. Elastoslide Model

In the preceding analysis, the MR fluid in the preyield condition is assumed to be incompressible. However, due to the compressibility of the fluid, the MR fluid in the preyield regime behaves like an elastic solid, such that the MR damper exhibits a strong force-velocity hysteresis at low velocity. Thus, the preyield stiffness must be considered in a physically motivated damper model. In the RDES model, the series combination of a stiff spring and the slide will be proven reasonable to reflect the preyield behavior of the MR fluid, and the coupling between the spring and the rate-dependent slide can be solved by efficient mathematical algorithms.

To demonstrate the efficiency of the elastoslide model in describing the yield behavior of MR fluids, instead of the rate-dependent slide, a Coulomb slide is used in series with a linear leading spring. The stiffness of the leading spring is denoted by k, and the maximum controllable yield force of the Coulomb, or slip slide, is N. Apparently, when the spring stiffness becomes large, the elastoslide model behaves exactly the same as the nonlinear Bingham-plastic model. When cycled between fixed deflection limits, the elastoslide model has a force-deflection diagram similar to that shown in Fig. 7. Upon initial loading, the spring force increases linearly with the applied displacement until it reaches the maximum slide yield force; that is,

$$f = kx, \quad \dot{x} > 0, 0 \le x \le \frac{N}{k}, \quad f = N, \quad \dot{x} > 0, x \ge \frac{N}{k} \tag{13}$$

If the direction of loading is reversed after the MR fluid has yielded, the force-deflection relation will become

$$f = N - k(A - x), \qquad \dot{x} < 0, A - 2\frac{N}{k} \le x \le A,$$
$$f = -N, \qquad \dot{x} < 0, x \le A - 2\frac{N}{k} \tag{14}$$

where A is the amplitude of the displacement excitation. An expression similar to Eq. (14) is obtained when the excitation reaches the minimum deflection and is reversed again so that $\dot{x} > 0$. This process continues until the excitation is stopped. The simulated force-displacement hysteresis by the elastoslide model is shown in Fig. 7 at two different amplitudes, and the arrows on the solid line show the loading direction of the model. Compared with the experimental force-displacement hysteresis of the MR damper, the elastoslide model captures the major characteristics of the MR-fluid yield behavior under sinusoidal excitation, except that the hysteresis around the maximum velocity cannot be described by the Coulomb slide. The Coulomb slide is an approximation of real MR-fluid yield behavior, and the amplitude of the excitation must be known a priori. However, this problem can be easily solved if the Coulomb slide is replaced with a rate-dependent slide.

Physically, the series combination of a spring and a rate-dependent slide can analytically describe the yield behavior of the MR fluid in the valve. Before the MR damper is subjected to excitation, the MR fluid in the flow gap consists of chain structures, due to an applied magnetic field. Thus, it behaves like a elastic solid, due to its compressibility. Because the damper piston is excited by an initial displacement excitation, the spring force due to the elastic MR solid increases with displacement. At the same time, the movement of the piston induces the partial breakdown of the chain structures and the piston bleed reduces the spring force. In this phase, the MR fluid flows like a plug. After all of the chain structures are broken, the MR fluid is totally yielded and the imagined spring is not extended any more, such that the damper demonstrates a viscous damping behavior. As the loading is reversed, the direction of the MR flow is also reversed and a similar yield process is repeated.

In addition to the rate-dependent elastoslide element, a viscous damping element is added in parallel in the RDES model, because the postyield behavior of the MR damper is similar to a viscous damper. Meanwhile, a soft parallel spring is introduced to account for the effect of the stiffness of the accumulator in the damper. Thus, as shown in Fig. 5, the MR damper can be represented by the mechanism-based rate-dependent elastoslide model. The parameters in the model need to be identified, including N, v_r, and p for the rate-dependent slide, k for the leading elastospring, c for the viscous damping, and k_0 for the accumulator stiffness.

C. Determine Model Parameters Using Hysteresis Data

As stated in the comparison of the elastoslide model with the Bingham-plastic model, the model parameters could be determined from the MR-fluid and damper-geometry data. On the other hand, when these data are not available, the model parameters can be identified to fit the predicted or modeled response to the experimentally measured response from either quasi-steady or dynamic tests. In this study, we take a system identification perspective, so that we use force-displacement and force-velocity hysteresis cycles obtained from the MR damper under single-frequency sinusoidal excitations to identify the model parameters.

The analysis of the Coulomb elastoslide showed that the initial loading curve from the preyield to the postyield phase can provide estimates of the yield force N and the preyield stiffness k. Therefore, the first step to determine the model parameters is to build a virtual initial loading curve from steady-state hysteresis-cycle diagrams. Because the maximum force corresponds to the maximum displacement (zero velocity) for a Coulomb friction slide, the virtual initial loading curve can be obtained from the force-displacement hysteresis by locating the damper force at zero velocity for each sinusoidal loading amplitude, as shown in Fig. 8a. Thus, the effect of the viscous damping force is eliminated. The loading curve is easily optimized by an exponent function as

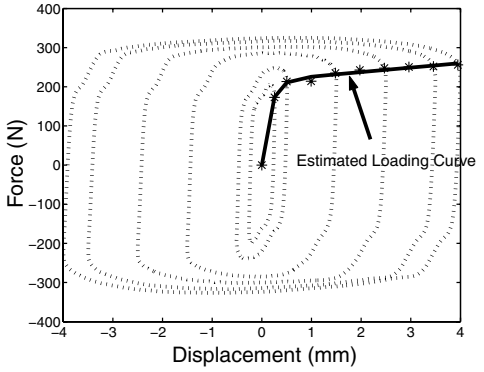

a) Force-displacement diagram

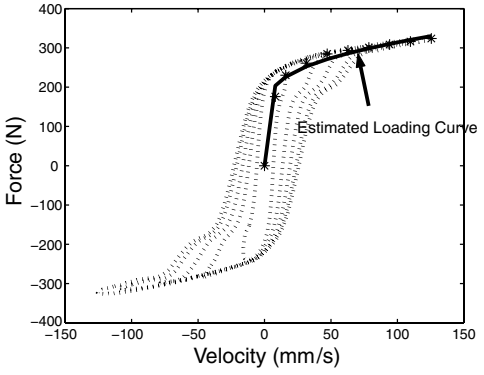

b) Force-velocity diagram

Fig. 8 Identified initial loading curve.

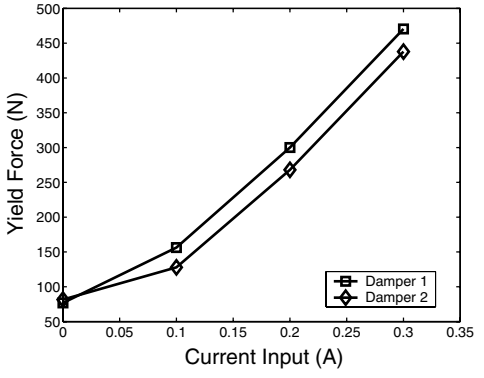

a) Yield force

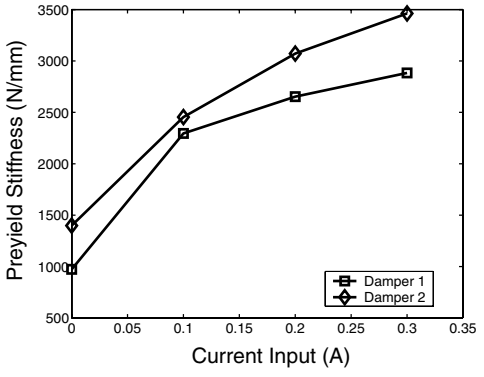

b) Preyield stiffness

Fig. 9 Model parameters (yield force and preyield stiffness) as a function of current.

Table 2 Model parameters

Parameter	Value	Current, A
N, N	76.75	0
	470.48	0.3
k, N/mm	973.13	0
	2883.35	0.3
c, N × s/mm	0.25	
k_0, N/mm	3	
v_r, mm/s	50	
n	7	

$$F_{\text{dis}} = N(1 - e^{-\frac{k}{N}x}) + k_0 x \tag{15}$$

from which the stiffness $k + k_0$ is the slope of the loading curve at zero displacement, k_0 is the slope of the postyield region of the loading curve, and N is the yield force. Because the slope of the loading curve at small displacements is sensitive to the hysteresis curve at the smallest amplitude, the determination of the preyield stiffness k is also referred to the force-displacement slope around maximum displacement. Because the Coulomb behavior is an idealization of the RDES model, the virtual initial loading curve determined from the preceding method is revised by judiciously adjusting the yield force in reference to the force-velocity hysteresis to include the effect of the rate-dependent slide and the postyield viscous damping.

To determine parameters v_r and p in the rate-dependent elastoslide and the postyield viscous damping c, a force-velocity loading curve is constructed from experimental force-velocity hysteresis diagrams. As shown in Fig. 8b, the damper force at zero displacement is used to obtain the virtual loading curve because, ideally, the effect of the stiffness is excluded at zero displacement. Without the stiffness, it is known from the RDES model structure that the force-velocity relationship of the damper can be described by

$$F_{\text{vol}} = N\left(\frac{v}{v_r}\right)^{\frac{1}{p}} + cv \tag{16}$$

Thus, by optimizing the loading curve using this function and the determined yield force, v_r, p, and c can be identified. However, determination of p is a tradeoff process. Physically, the index p should be large enough so that the postyield damping will not overpredicted, but a larger index will lead to a stiffer system mathematically. Consideration must be taken carefully into account in the choice of p.

A group of single-frequency hysteresis cycles at different excitation amplitudes (0.25–4.0 mm) is used to determine the model parameters at a fixed frequency and applied current. The model parameters are determined independently at three different frequencies (2.5, 5, and 7.5 Hz) and at four different currents (0.0, 0.1, 0.2, and 0.3 A). Because the damping mechanism for the MR damper is mainly due to the yield process of the MR fluid, the model parameters demonstrate weak dependence on three frequencies. In a

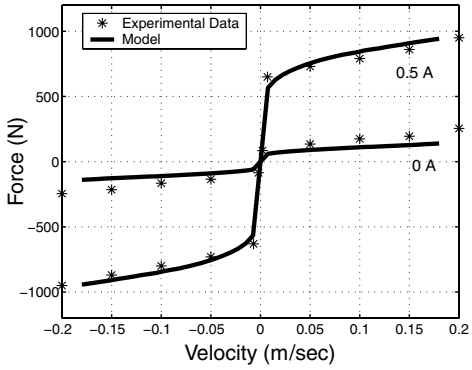

Fig. 10 Quasi-steady behavior of the model.

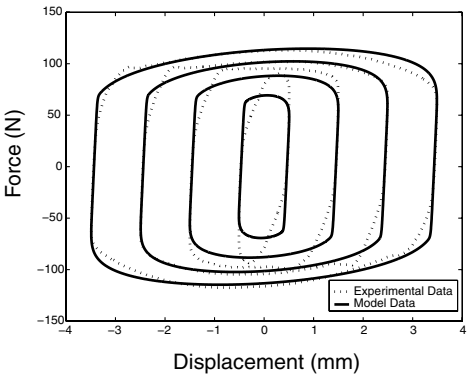

a) Force-displacement diagram

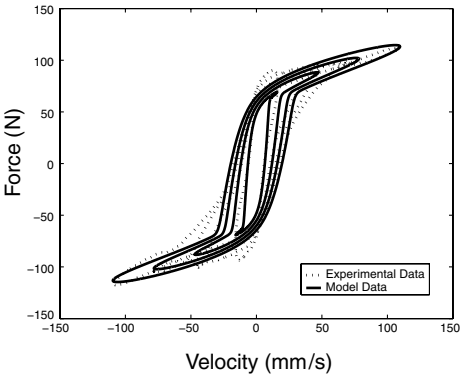

b) Force-velocity diagram

Fig. 11 Model fit at 5 Hz and 0 A.

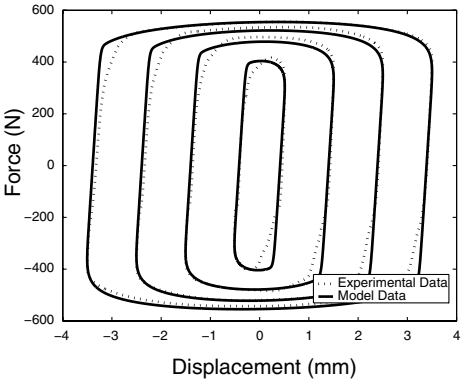

a) Force-displacement diagram

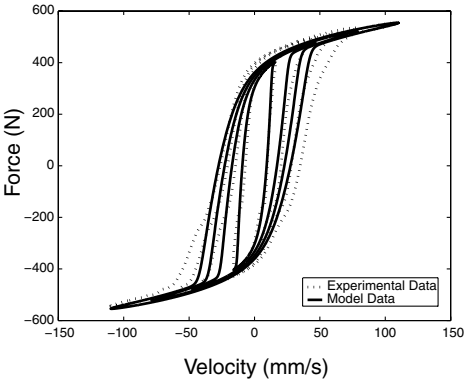

b) Force-velocity diagram

Fig. 12 Model fit at 5 Hz and 0.3 A.

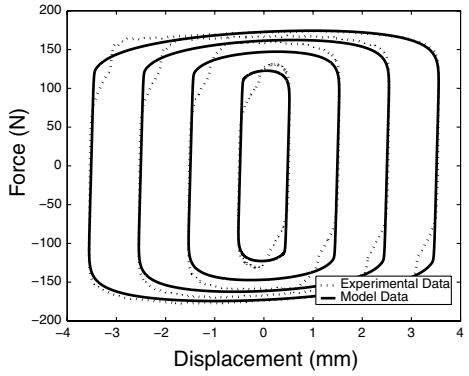

a) Force-displacement diagram

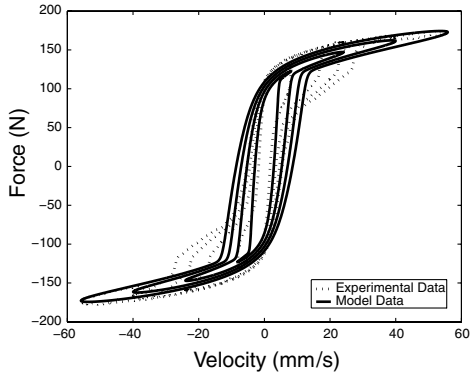

b) Force-velocity diagram

Fig. 13 Model fit at 2.5 Hz and 0.1 A.

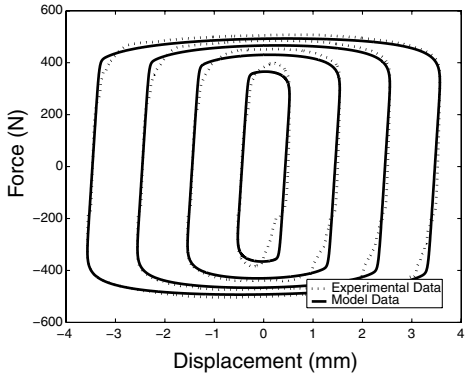

a) Force-displacement diagram

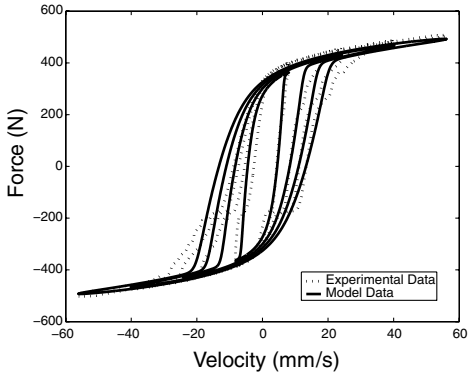

b) Force-velocity diagram

Fig. 14 Model fit at 2.5 Hz and 0.3 A.

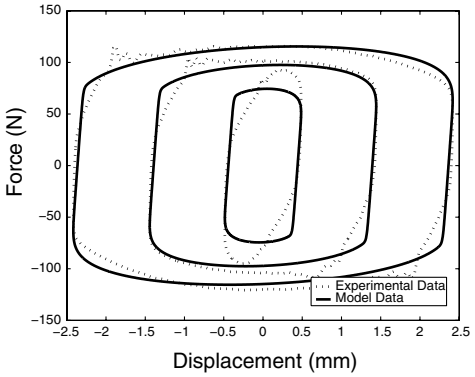

a) Force-displacement diagram

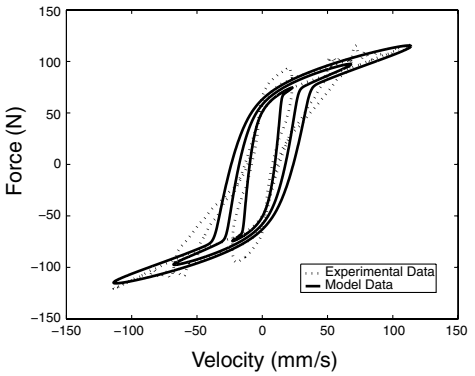

b) Force-velocity diagram

Fig. 15 Model fit at 7.5 Hz and 0 A.

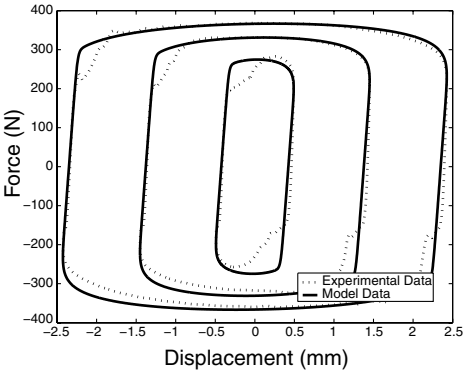

a) Force-displacement diagram

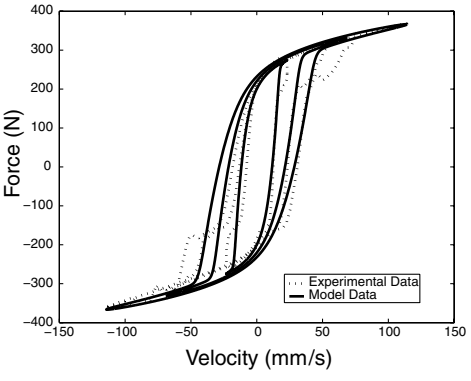

b) Force-velocity diagram

Fig. 16 Model fit at 7.5 Hz and 0.2 A.

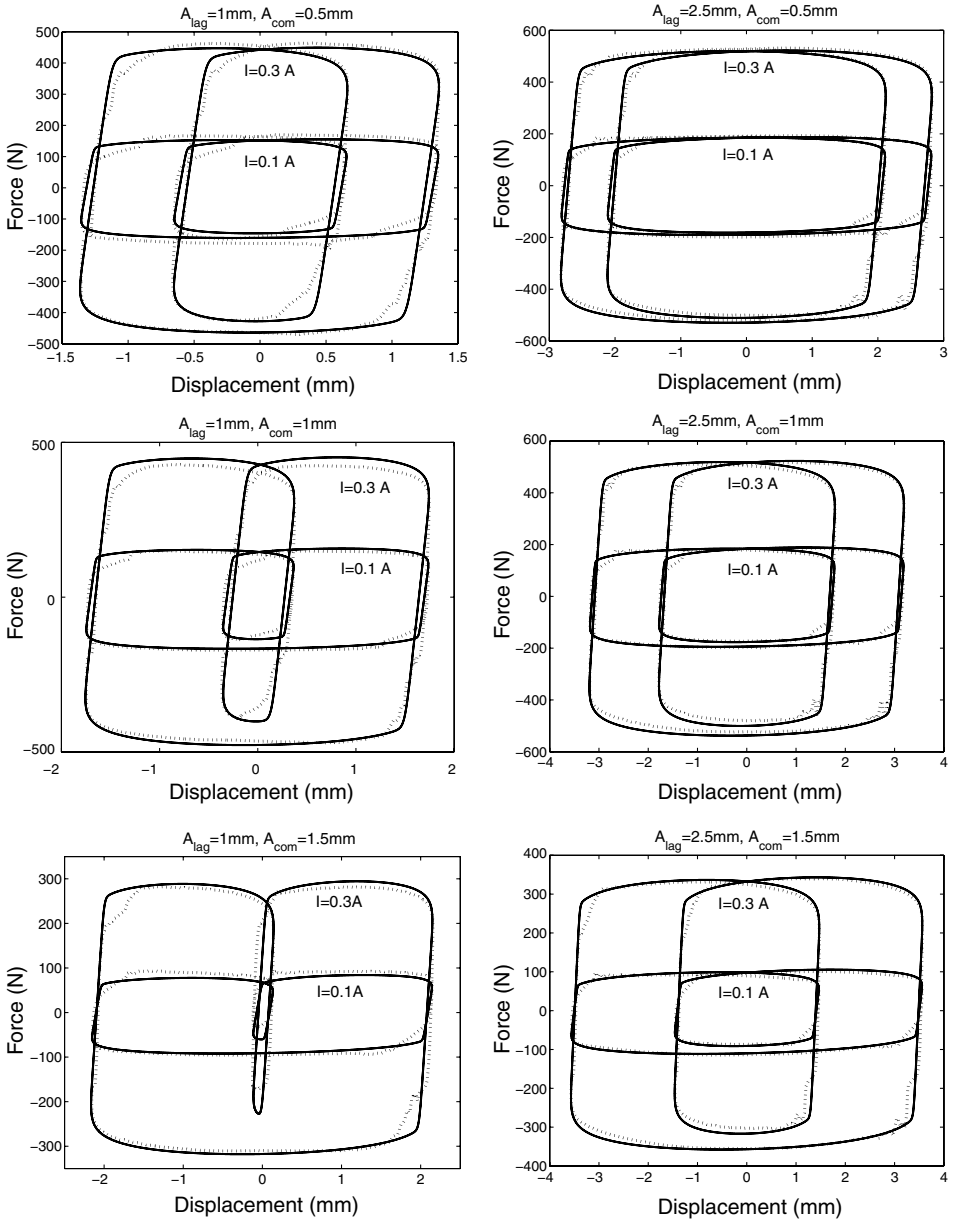

Fig. 17 Dual-frequency modeling at 5.0 and 2.5 Hz.

moderate-frequency range, the model parameters are fixed by an averaging process. The dependence of the parameters on the applied current is also studied. Two major parameters, N and k, are a function of current, as shown in Fig. 9. The modeling results for two MR dampers demonstrate the same trend as the applied current changes from 0 to 0.3 A. The yield force increases sharply with the applied current, because the magnetic field is not saturated yet. This result is consistent with the result in [21]. Comparatively, the preyield stiffness varies much more slowly with applied current. As the applied current increases, the preyield stiffness converges to a constant value. The other four parameters (k_0, v_r, p and c) are not varied as the current is changed.

The resulting modeling parameters are given in Table 2. Note that the field-off yield force is not zero, and it can be interpreted by the effect of the residual magnetization in the MR valve and the friction of the damper assembly. Because the rate-dependent elastoslide model is a physically motivated model, the determination of model parameters (especially for N, k, c, and k_0) is a process to capture the relationship between damper mechanism and damper behavior. Either quasi-steady or dynamic test data can be used to evaluate the model parameters. The method for parameter determination used in this study is only an option, and it does not require fitting the hysteresis response of the model to the experimentally measured response.

IV. Model Validation

Because the rate-dependent elastoslide model is a time-domain model, it can be used for both quasi-steady and dynamic analyses. In this section, the numerical implementation of the model is developed, and the quasi-steady and dynamic modeling results are validated by the experimental data.

A. Numerical Fulfillment of the Model

Numerically, in the rate-dependent elastoslide model, the internal displacement x_0 of the rate-dependent slide is a coupling variable between the elastic stiffness and the slide. For a rate-dependent elastoslide element, as shown in Fig. 5, as displacement excitation x is applied, the resistant force of the elastoslide element is given by

$$F = k(x - x_0) = N\left(\frac{\dot{x}_0}{v_r}\right)^{\frac{1}{p}} \tag{17}$$

the coupling displacement x_0 is given by

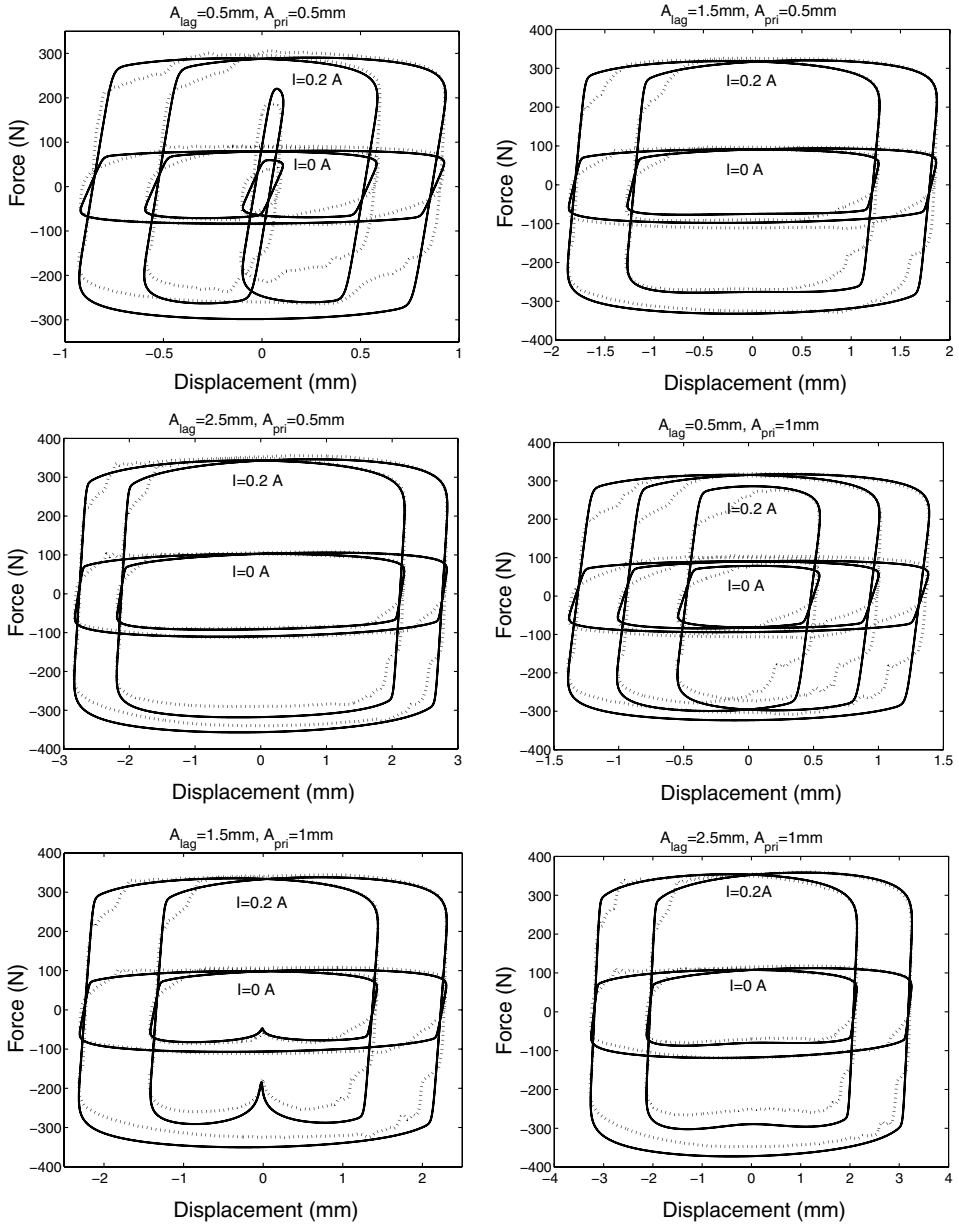

Fig. 18 Dual-frequency modeling at 5.0 and 7.5 Hz.

$$\frac{\dot{x}_0}{v_r} = \left[\frac{k}{N}(x - x_0)\right]^p \tag{18}$$

This is a typical well-posed initial-value problem, and numerical solution for this differential equation can be obtained given an initial condition. The simplest way to guarantee a stable solution for stiff initial-value problems is to adopt a predictor–corrector approach, with the corrector iterated to convergence [22]. In this application, the numerical algorithm for Eq. (18) is based on the Adams–Bashforth four-step method as the predictor and one iteration of the Adams–Moulton three-step method as the corrector, with the starting values obtained from the Runge–Kutta method of order four [22]. In accordance with the ratio of yield force and stiffness k/N in the current MR damper and an appropriate choice of p, a stable and fast solution can be given by the Adams–Bashforth–Moulton method using limited time steps. Including the postyield viscous damping and accumulator stiffness, the total MR damper model force is given by

$$F^{\mathrm{MR}} = k(x - x_0) + c\dot{x} + k_0 x \tag{19}$$

In addition, the model response can be solved using a MATLAB ordinary differential equation (ODE) solver. Because the internal velocity $\dot{x_0}$ is the function of internal displacement x_0 and displacement excitation x, as shown in Eq. (18), the internal displacement can be solved using ODE23, and the model force is further developed by Eq. (19). Similarly, because the MR damper is incorporated in a mass-spring system with damping, the motion of equation of the system is transferred to the first-order state-space form and the system free vibration and forced response can be obtained using the ODE solver. For instance, a 1-DOF mass-spring system with the MR damper can be expressed in state-space form as

$$\begin{aligned} \dot{x} &= \dot{x} \\ \ddot{x} &= \frac{F(t)}{M} - \frac{K}{M}x - \frac{1}{M}[k(x - x_0) + c\dot{x} + k_0 x], \\ \dot{x}_0 &= \left[\frac{k}{N}(x - x_0)\right]^p v_r \end{aligned} \tag{20}$$

where M and K are the mass and spring of the system, respectively, and $F(t)$ is a forced loading on the system. Thus, given a initial condition, the system response will be easily solved. Using the same

ODE solver, the RDES model can also be applied in the MATLAB Simulink program such that control simulations using MR damper can be easily realized.

B. Experimental Validation

Because the RDES model is a time-domain model, the quasi-steady and steady-state hysteretic modeling results are used to validate the model. For quasi-steady study, the model response is calculated when the damper model is applied by a displacement excitation with a constant velocity. Figure 10 shows the analytical damper force under varied velocities and applied currents in comparison with the experimental data. The experimental data are provided by the Lord's damper performance data sheet,[‡] in which the offset force due to the accumulator is excluded. As shown in the figure, the damper force due to a steady shaft velocity predicted by the RDES model demonstrates similar field-dependent characteristics demonstrated by the experimental result.

It is more important to understand the damper behavior when the damper is applied by sinusoidal excitations, because the damper is mainly used in a dynamic system to dissipate energy. Single-frequency and dual-frequency experimental results are used to evaluate the fidelity of the rate-dependent elastoslide model. For single-frequency data, modeling and experimental results are compared using both force-displacement and force-velocity hysteresis cycles. Figures 11 and 12 show the force-displacement and force-velocity hysteresis cycles at 5 Hz. The applied current is 0 and 0.3 A, respectively. Clearly, the modeling results correlate very well with the experimental results; especially, the proposed model captures the amplitude-dependent damping behavior of the MR damper. The main reason for the irregular curve at the upper-left and lower-right corners of the experimental force-displacement diagram is due to the loose fit of the insert-pin connection between the MR damper and the fixture connected to the material testing machine. The single-frequency modeling results at 2.5 Hz are shown in Figs. 13 and 14. The modeling results at 7.5 Hz are shown in Figs. 15 and 16. From these single-frequency modeling results, it can be concluded that the rate-dependent elastoslide model can predict the damper response very well in a moderate-frequency range.

For dual-frequency data, the force-displacement diagram is used to evaluate the MR damper model. The modeling and experimental results at various combinations of dual-frequency amplitudes and currents are shown in Figs. 17 and 18. The modeling results for combination of 2.5 and 5 Hz are shown in Fig. 17, in which A_{lag} is the amplitude of the sinusoidal signal at 5 Hz and A_{com} is the amplitude of the signal at 2.5 Hz. There are six combinations of amplitudes for A_{lag} and A_{com}, and the results at two different currents demonstrate controllability of the MR damper. The dual-frequency data at 7.5 and 5 Hz are shown in Fig. 18. The correlation results in both dual-frequency combinations show that the rate-dependent elastoslide model performs quite well in predicting the dual-frequency behavior at a broad amplitude and frequency range.

The fidelity of the rate-dependent elastoslide model over a broad amplitude and moderate-frequency range is justified by the good correlation with experimental single- and dual-frequency test data. Because the proposed model is a time-domain model, it also can be used to predict damper behavior under quasi-steady or complex dynamic loading conditions. If the relationship between the model parameters and the applied current can be identified, then the damper model is capable of predicting the behavior of the MR damper for a continuously controlled magnetic field.

V. Conclusions

A rate-dependent elastoslide (RDES) model for a linear stroke MR damper was developed. The MR damping mechanism was developed using the Bingham model of MR fluids and the hydromechanical assumptions. The relationship between model parameters and damper mechanisms was studied. The model parameters were determined using identified virtual loading curves from force-displacement and force-velocity hysteresis data. A stable numerical method was chosen to predict the model response under various loading conditions. The predicted forced response correlated very well with the single- and dual-frequency experimental results. Significantly, the nonlinear amplitude-dependent behavior of the MR damper was described by this model with six constant parameters. The RDES model can be used in a variety of applications such as initial or forced-response analysis of the system using MR dampers and a wide range of proposed control strategies dealing with the MR damper.

In conclusion, the rate-dependent elastoslide model is a physically motivated time-domain model. It captures the nonlinearity of the MR damper using a simple model structure. Significantly, this modeling approach captures nonlinear amplitude- and frequency-dependent behavior of MR dampers using constant model parameters that can be determined by the properties of the MR fluids and damper-geometry data.

[‡]Data available online at http://www.lordfulfillment.com/upload/DS7017.pdf [retrieved 21 January 2008].

References

[1] Wereley, N. M., and Pang, L., "Nondimensional Analysis of Semi-Active Electrorheological and Magnetorheological Dampers Using Approximate Parallel Plate Models," *Smart Materials and Structures*, Vol. 7, No. 5, 1998, pp. 732–743. doi:10.1088/0964-1726/7/5/015

[2] Lee, D. Y., and Wereley, N. M., "Quasi-steady Herschel–Bulkley Analysis of Electro- and Magneto-Rheological Flow Mode Dampers," *Journal of Intelligent Material Systems and Structures*, Vol. 10, No. 10, 1999, pp. 761–769. doi:10.1106/E3LT-LYN6-KMT2-VJJD

[3] Lee, D. Y., Choi, Y. T., and Wereley, N. M., "Performance Analysis of ER/MR Impact Damper Systems Using Herschel–Bulkley Model," *Journal of Intelligent Material Systems and Structures*, Vol. 13, Nos. 7–8, 2002, pp. 525–531. doi:10.1106/104538902031061

[4] Phillips, R. W., "Engineering Application of Fluids with a Variable Yield Stress," Ph.D. Thesis, Department of Mechanical Engineering, Univ. of California at Berkeley, Berkeley, CA, 1969.

[5] Pang, L., Kamath, G. M., and Wereley, N. M., "Analysis and Testing of a Linear Stroke Magnetorheological Damper," *AIAA/ASME/ASCE/AHS/ASC Structures, Structural Dynamics and Materials Conference*, Vol. 4, AIAA, Reston, VA, 1998, pp. 2841–2856.

[6] Snyder, R. A., Kamath, G. M., and Wereley, N. M., "Characterization and Analysis of Magnetorheological Damper Behavior Under Sinusoidal Loading," *AIAA Journal*, Vol. 39, No. 7, July 2001, pp. 1240–1253.

[7] Williams, S., Rigby, S. G., Sproston, J. L., and Stanway, R., "Electrorheological Fluids Applied to an Automotive Engine Mount," *Journal of Non-Newtonian Fluid Mechanics*, Vol. 47, June 1993, pp. 221–238. doi:10.1016/0377-0257(93)80052-D

[8] Stanway, R., Sproston, J. L., and EI-Wahed, A. K., "Application of Electrorheological Fluids in Vibration Control: A Survey," *Smart Materials and Structures*, Vol. 6, No. 3, 1997, pp. 351–358. doi:10.1088/0964-1726/6/3/012

[9] Choi, Y. T., Lionel, B., and Wereley, N. M., "Nondimensional Analysis of Electrorheological Dampers Using an Eyring Constitutive Relationship," *Journal of Intelligent Material Systems and Structures*, Vol. 16, No. 5, 2005, pp. 383–394. doi:10.1177/1045389X05050529

[10] Wereley, N. M., Pang, Li, and Kamath, G. M., "Idealized Hysteresis Modeling of Electrorheological and Magnetorheological Dampers," *Journal of Intelligent Material Systems and Structures*, Vol. 9, No. 8, 1998, pp. 642–649.

[11] Choi, Y. T., Wereley, N. M., and Jeon, Y. S., "Semi-Active Vibration Isolation Using Magnetorheological Isolators," *Journal of Aircraft*, Vol. 42, No. 5, 2005, pp. 1244–1251.

[12] Choi, S. B., Lee, S. K., and Park, Y. P., "A Hysteresis Model for the Field-Dependent Damping Force of a Magnetorheological Damper," *Journal of Sound and Vibration*, Vol. 245, No. 2, 2001, pp. 375–383. doi:10.1006/jsvi.2000.3539

[13] Kamath, G. M., Wereley, N. M., and Jolly, M. R., "Characterization of Magnetorheological Helicopter Lag Dampers," *Journal of the American Helicopter Society*, Vol. 44, No. 3, 1999, pp. 234–248.

[14] Gamota, D. R., and Filisko, F. E., "Dynamic Mechanical Studies of Electrorheological Materials: Moderate Frequencies," *Journal of Rheology (New York)*, Vol. 35, No. 3, 1991, pp. 399–425. doi:10.1122/1.550221

[15] Wen, Y. K., "Method for Random Vibration of Hysteretic Systems," *Journal of the Engineering Mechanics Division, American Society of Civil Engineers*, Vol. 102, No. 2, 1976, pp. 249–263.

[16] Spencer, B. F. Jr., Dyke, S. J., Sain, M. K., and Carlson, J. D., "Phenomenological Model of a Magnetorheological Damper," *Journal of Engineering Mechanics*, Vol. 123, No. 3, 1997, pp. 230–238. doi:10.1061/(ASCE)0733-9399(1997)123:3(230)

[17] Wang, X. J., and Gordaninejad, F., "Flow Analysis and Modeling of Field-Controllable, Electro- and Magneto-Rheological Fluid Dampers," *Journal of Applied Mechanics*, Vol. 74, No. 1, 2007, pp. 13–22. doi:10.1115/1.2166649

[18] Hong, S. R., Choi, S. B., Choi, Y. T., and Wereley, N. M., "Comparison of Damping Force Models for an Electrorheological Fluid Damper," *International Journal of Vehicle Design*, Vol. 33, Nos. 1–3, 2003, pp. 17–35. doi:10.1504/IJVD.2003.003650

[19] Gavin, H. P., Hanson, R. D., and Filisko, F. E., "Electrorheological Dampers, Part 1: Analysis and Design," *Journal of Applied Mechanics*, Vol. 63, No. 3, 1996, pp. 669–675.

[20] Hu, W., and Wereley, N. M., "Hybrid Magnetorheological Elastomeric Lag Dampers for Helicopter Stability Augmentation," *59th Annual Forum of the American Helicopter Society*, AHS International, Alexandria, VA, 6–8 May 2003, pp. 1001–1012.

[21] Li, W. H., Yao, G. Z., Chen, G., Yeo, S. H., and Yap, F. F., "Testing and Steady State Modeling of a Linear MR Damper Under Sinusoidal Loading," *Smart Materials and Structures*, Vol. 9, No. 1, 2000, pp. 95–102. doi:10.1088/0964-1726/9/1/310

[22] Faires, J. D., and Burden, R., *Numerical Methods*, Brooks/Cole, Pacific Grove, CA, 1998.